

1 A systematic examination of the relationships between CDOM and
2 DOC in inland waters in China

3 Kaishan Song¹, Ying Zhao^{1,2}, Zhidan Wen¹, Chong Fang^{1,2}, Yingxin Shang¹

4 ¹Northeast Institute of Geography and Agroecology, CAS, Changchun, 130102, China

5 ² University of Chinese Academy of Sciences, Beijing 100049, China

6 Corresponding author's E-mail: songks@iga.ac.cn; Tel: 86-431-85542364

7
8 **Abstract:** Chromophoric dissolved organic matter (CDOM) plays a vital role in the
9 biogeochemical cycle in aquatic ecosystems. The relationship between CDOM and
10 dissolved organic carbon (DOC) has been investigated, and the significant relationship
11 lays the foundation for the estimation of DOC using remotely sensed imagery data. The
12 current study examined the samples from freshwater lakes, saline lakes, rivers and
13 streams, urban water bodies, and ice-covered lakes in China for tracking the variation
14 of the relationships between DOC and CDOM. The regression model slopes for DOC
15 versus $a_{CDOM}(275)$ ranged from extreme low 0.33 (highly saline lakes) to 1.03 (urban
16 waters) and 3.01 (river waters). The low values were observed in saline lake waters and
17 waters from semi-arid or arid regions where strong photo-bleaching is expected due to
18 less cloud cover, longer water residence time and daylight hours. In contrast, high
19 values were found in waters developed in wetlands or forest in Northeast China, where
20 more organic matter was transported from catchment to waters. The study also
21 demonstrated that closer relationships between CDOM and DOC were revealed when
22 $a_{CDOM}(275)$ were sorted by the ratio of $a_{CDOM}(250)/a_{CDOM}(365)$, which is a measure for

23 the CDOM absorption with respect to its composition, and the determination of
24 coefficient of the regression models ranged from 0.79 to 0.98 for different groups of
25 waters. Our results indicated the relationships between CDOM and DOC are variable
26 for different inland waters, thus models for DOC estimation through linking with
27 CDOM absorption need to be tailored according to water types.

28

29 **Keywords:** Absorption, CDOM, DOC, regression slope, saline water, fresh water

30

31 **1. Introduction**

32 Inland waters play a disproportional role for the global carbon cycling with respect to
33 carbon transportation, transformation and carbon storage (Tranvik et al., 2009;
34 Raymond et al., 2013; Verpoorter et al., 2014; Yang et al., 2015). However, the amount
35 of dissolved organic carbon (DOC) stored in the inland waters is still unclear or the
36 uncertainty is still needed to be evaluated (Tranvik et al., 2009). Determination DOC
37 concentration is straightforward through field sampling and laboratory analysis
38 (Findlay and Sinsabaugh, 2003). However, there are millions of lakes in the world, and
39 many of them are remote and inaccessible, making it impossible to evaluate DOC
40 concentration using routine approach (Cardille et al., 2013; Brezonik et al., 2015; Pekel
41 et al., 2016). Researchers have found that remote sensing might provide a promising
42 tool for quantification of DOC of inland waters at large scale through linking DOC with
43 chromophoric dissolved organic matter (CDOM), particularly for inland waters
44 situating in remote area with less accessibility (Tranvik et al., 2009; Kutser et al., 2015;
45 Brezonik et al., 2015).

46 As one of the optically active constituents (OACs) in waters, CDOM can be
47 estimated through remotely sensed signals (Yu et al., 2010; Kutser et al., 2015), and is
48 acted as a proxy in many regions for the amount of DOC in the water column. As shown
49 in Fig.1, CDOM and DOC in the aquatic ecosystems are mainly originated from natural
50 external (allochthonous) and internal (autochthonous) sources, in addition to directly
51 discharge from anthropogenic activities (Zhou et al., 2016). Generally, the
52 autochthonous CDOM is essentially originated from algae and macrophytes, and

53 mainly consists of various compounds of low molecular weights (Findlay and
54 Sinsabaugh, 2003; Zhang et al., 2010). While, the allochthonous CDOM is mainly
55 derived from the surrounding terrestrial ecosystems, and it comprises a continuum of
56 small organic molecules to highly polymeric humic substances. In terms of CDOM
57 originating from anthropogenic sources, it contains fatty acid, amino acid and sugar,
58 thus the composition of CDOM is more complex than that from natural systems (Zhou
59 et al., 2016; Zhao et al., 2016a). Hydrological factors also affect the DOC and CDOM
60 characteristic and particularly, the discharge, catchment area, land use and travel time
61 are the important ones (Neff et al., 2006; Spencer et al., 2012).

62 **[Insert Fig.1 about here]**

63 CDOM is a light-absorbing constituent, which is partially responsible for the color
64 in waters (Bricaud et al., 1981; Reche et al., 1999; Babin et al., 2003). The chemical
65 structure and origin of CDOM can be characterized by its absorption coefficients
66 ($a_{CDOM}(\lambda)$) and spectral slopes (De Haan and De Boer, 1987; Helms et al., 2008).
67 Weishaar et al. (2003) has proven that the carbon specific absorption coefficient at 254
68 nm, e.g., $SUVA_{254}$ is a good tracer for the aromaticity of humic acid in CDOM, while
69 the ratio of CDOM absorption at 250 to 365 nm, i.e., $a_{CDOM}(250)/a_{CDOM}(365)$, herein,
70 M value, has been successfully used to track the variation in DOM molecular weight
71 (De Haan and De Boer, 1987). Biodegradation and photodegradation are the major
72 processes to determine the transformation and composition of CDOM (Findlay and
73 Sinsabaugh, 2003; Zhang et al., 2010), which ultimately affect the relationship between
74 DOC and CDOM (Spencer et al., 2012; Yu et al., 2016). With prolonged sunlight

75 radiation, some of the colored fraction of CDOM is lost by the photobleaching
76 processes (Miller et al., 1995; Zhang et al., 2010), which can be measured by the light
77 absorbance decreasing at some specific (diagnostic) wavelength, e.g., 250, 254, 275,
78 295, 360 and 440 nm.

79 It should be noted that $a_{CDOM(440)}$ is usually used by remote sensing community
80 due to this wavelength is overlapped with pigment absorption at 443 nm, thus reporting
81 $a_{CDOM(440)}$ has potential to improve chlorophyll-a estimation accuracy (Lee et al.,
82 2002). The relationship between CDOM and DOC varies since CDOM loses color while
83 the variation of DOC concentration is almost negligible. Saline or brackish lakes in the
84 arid or semi-arid regions are generally exposed to longer sunlight radiation, thus CDOM
85 absorbance decreases, while DOC is accumulated due to the longer residence time
86 (Curtis and Adams, 1995; Song et al., 2013; Wen et al., 2016). Compared to
87 photodegradation of CDOM, the biodegradation processes by microbes are much more
88 complicated, and extracellular enzymes are the key factors required to decompose the
89 high-molecular-weight CDOM into low-molecular-weight substrates (Findlay and
90 Sinsabaugh, 2003). With compositional change, the absorption feature of CDOM and
91 its relation to DOC varies correspondingly, and the relationship between CDOM and
92 DOC needs to be systematically examined (Gonnelli et al., 2013). In addition, the
93 $SUVA_{254}$ and M value may be used to classify CDOM into different groups and enhance
94 the relationship with DOC based on CDOM absorption grouping.

95 Some studies have investigated the spatial and seasonal variations of CDOM and
96 DOC in ice free season in lakes, rivers and oceans (Vodacek et al., 1997; Neff et al.,

97 2006; Stedmon et al., 2011; Brezonik et al., 2015), but less is known about saline lakes
98 (Song et al., 2013; Wen et al., 2016). Even less is known about urban waters influenced
99 by sewage effluent and waters with ice cover in winter (Belzile et al., 2002; Zhao et al.,
100 2016b). A significant relationship between CDOM and DOC was observed in the Gulf
101 of Mexico, and stable regression model was established between DOC and $a_{CDOM}(275)$
102 and $a_{CDOM}(295)$ (Fichot and Benner, 2011). Similar results were also found in other
103 estuaries along a salinity gradient, for example the Baltic Sea surface water (Kowalczyk
104 et al., 2010) and the Chesapeake Bay (Le et al., 2013). However, Chen et al. (2004)
105 found that the relationship between CDOM and DOC was not conservative due to
106 estuarine mixing or photo-degradation. Similar arguments were raised for Congo River
107 and waters across mainland USA (Spencer et al., 2009, 2012). In addition, seasonal
108 variations were observed in some studies due to the mixing of various endmembers of
109 CDOM from different terrestrial ecosystems and internal source (Zhang et al., 2010;
110 Spencer et al., 2012; Yu et al., 2016; Zhou et al., 2016).

111 As demonstrated in Fig.1, several factors influence the association between DOC
112 and CDOM, thus the relationship between DOC and CDOM may vary with respect to
113 their origins, photo- or bio-degradations, and hydrological features, which is worth of
114 systematic examination. In this study, the characteristics of DOC and CDOM in
115 different inland waters across China were examined to determine the spatial feature
116 associated with landscape variations, hydrologic conditions and saline gradients. The
117 objectives of this study are to: 1) examine the relationship between CDOM and DOC
118 concentrations across a wide range of waters with various physical, chemical and

119 biological conditions, and 2) develop a model for the relationship between DOC and
120 CDOM based on the sorted CDOM absorption feature, e.g., the M values with aiming
121 to improve the regression modeling accuracy.

122 **2. Materials and Methods**

123 The dataset is composed of five subsets of samples collected from various types of
124 waters across China (Table 1, Fig.2), which encompassed a wide range of DOC and
125 CDOM. The first dataset (n = 288; from early spring 2009 to late October 2014)
126 includes samples collected in freshwater lakes and reservoirs during the growing season
127 with various landscape types. The second dataset (n = 345; from early spring 2010 to
128 late mid-September 2014) includes samples collected in brackish to saline water bodies.
129 The third dataset (n = 322; from early May 2012 to late July 2015) includes samples
130 collected in rivers and streams across different basins in China. In addition, 69 samples
131 were collected from three sections along the Songhua Rive, the Yalu and the Hunjiang
132 River during the ice free period in 2015 to examine the impact of river flow on the
133 relationship between DOC and CDOM (see Fig.S1 for location). The fourth dataset (n
134 = 328; from 2011 to 2014 in the ice frozen season) includes samples collected in
135 Northeast China in winter from both lake ice and underlying waters. The fifth dataset
136 (n = 221; from early May 2013 to mid-October 2014) collects samples in urban water
137 bodies, including lakes, ponds, rivers and streams, which were severely polluted by
138 sewage effluents. City maps and Landsat imagery data acquired in 2014 or 2015 were
139 used to delineate urban boundaries with ArcGIS 10.0 (ESRI Inc., Redlands, California,
140 USA), and water bodies in these investigated cities constrained by urban boundaries

141 were considered as urban water bodies. The sampling dates, water body names and
142 locations of other types of water bodies were provided in supplementary Table S1-4.

143 **[Insert Fig.2 about here]**

144 **2.1 Water quality determination**

145 Water samples were collected approximately 0.5m below the water surface at each
146 station, generally locating in the middle of water bodies. Water samples were collected
147 in two 1 L amber HDPE bottles, and kept in coolers with ice packs in the field and kept
148 in refrigerator at 4°C after shipping back to the laboratory. All samples were
149 preprocessed (e.g., filtration, pH and electrical conductivity (EC) determination) within
150 two days in the laboratory. Water salinity was measured using DDS-307 EC meter
151 ($\mu\text{S}/\text{cm}$) at room temperature ($20\pm 2^\circ\text{C}$) in the laboratory and converted to *in situ* salinity,
152 expressed in practical salinity units (PSU). Water samples were filtered using Whatman
153 cellulose acetone filter with pore size of 0.45 μm . Chlorophyll-a (Chl-a) was extracted
154 and concentration was measured using a Shimadzu UV-2600PC spectrophotometer, the
155 details can be found in Jeffrey and Humphrey (1975). Total suspended matter (TSM)
156 was determined gravimetrically using pre-combusted Whatman GF/F filters with
157 0.7 μm pore size, details can be found in Song et al. (2013). DOC concentrations were
158 measured by high temperature combustion (HTC) with water samples filtered through
159 0.45 μm Whatman cellulose acetone filters (Zhao et al., 2016a). The standards for
160 dissolved total carbon (DTC) were prepared from reagent grade potassium hydrogen
161 phthalate in ultra-pure water, while dissolved inorganic carbon (DIC) were determined
162 using a mixture of anhydrous sodium carbonate and sodium hydrogen carbonate. DOC

163 was calculated by subtracting DIC from DTC, both of which were measured using a
164 Total Organic Carbon Analyzer (TOC-VCPN, Shimadzu, Japan). Total nitrogen (TN)
165 was measured based on the absorption levels at 146 nm of water samples decomposed
166 with alkaline potassium peroxydisulfate. Total phosphorus (TP) was determined using
167 the molybdenum blue method after the samples were digested with potassium
168 peroxydisulfate (APHA, 1998). pH was measured using a PHS-3C pH meter at room
169 temperature (20±2°C).

170 **2.2 CDOM absorption measurement**

171 All water samples were filtered at low pressure at two steps: 1) filtered at low pressure
172 through a pre-combusted Whatman GF/F filter (0.7µm), and 2) further filtered through
173 pre-rinsed 25 mm Millipore membrane cellulose filter (0.22 µm). Absorption spectra
174 were obtained between 200 and 800 nm at 1 nm increment using a Shimadzu UV-
175 2600PC UV-Vis dual beam spectrophotometer (Shimadzu Inc., Japan) through a 1 cm
176 quartz cuvette (or 5 cm cuvette for ice melted water samples). Milli-Q water was used
177 as reference for CDOM absorption measurements. The Napierian absorption coefficient
178 (a_{CDOM}) was calculated from the measured optical density (OD) of samples using Eq.

179 (1):

$$180 \quad a_{CDOM}(\lambda) = 2.303[OD_{S(\lambda)} - OD_{(null)}] / \beta \quad (1)$$

181 where β is the cuvette path length (0.01 or 0.05m) and 2.303 is the conversion factor of
182 base 10 to base e logarithms. To remove the scattering effect from the limited fine
183 particles remained in the filtered solutions, a necessitated correction was implemented
184 by assuming the average optical density over 740–750 nm to be zero (Babin et al., 2003).

185 SUVA₂₅₄ and M values were calculated to characterize CDOM with respect to their
186 compositional features. In addition, a_{CDOM} was divided into different groups according
187 to M values by hierarchical cluster approach, which was performed in SPSS software
188 package with the pairwise distance between samples was measured by squared
189 Euclidean distance and the clusters were linked together by Ward's linkage method
190 (Ward Jr, 1963). The method has been applied to classify the waters into different types
191 according the remote sensing spectra (Vantrepotte et al., 2012; Shi et al., 2013).

192 **3. Results**

193 **3.1. Water quality characteristics**

194 Chl-a concentrations (46.44±59.71 µg/L) ranged from 0.28 to 521.12µg/L. TN and TP
195 concentrations were very high in fresh lakes, saline lakes and particularly urban water
196 bodies (Table 1). It is worth noting that Chl-a concentration was still high 7.3±19.7µg/L
197 even in ice-covered lakes in winter from Northeast China. Electric conductivity (EC)
198 and pH were high in the semi-arid and arid regions, and they were 1067-41000 µs/cm
199 and 7.1-11.4, respectively. Overall, waters were highly turbid with high TSM
200 concentrations (119.6 ± 131.4 mg/L), and apparent variations were observed for
201 different types of waters (Table 1). Hydrographic conditions exerted strong impact on
202 water turbidity and TSM concentration, thus these two parameters of river and stream
203 samples were excluded in this study (Table 1).

204 **[Insert Table 1 about here]**

205 **3.2. DOC concentrations in different types of waters**

206 DOC concentrations changed remarkably in the investigated waters (Table 1). The

207 concentration of DOC were low in rivers, and the lowest DOC concentrations were
208 measured in ice melting waters. It should be noted that large variations were observed
209 in water samples from rivers and streams (Table 2). Among the five types of waters,
210 relatively higher DOC concentrations, ranging from 2.3 to 300.6 mg/L, were found in
211 many saline lakes, in the Songnen Plain, the Hulunbuir Plateau and some areas in
212 Tibetan Plateau (see Fig.2 for location). However, some of saline lakes supplied by
213 snow melt water or ground water exhibited relatively lower DOC concentrations even
214 with high salinity. Compared with samples collected in growing seasons, higher DOC
215 concentrations (7.3-720 mg/L) were observed in ice-covered water bodies.

216 **[Insert Table 2 about here]**

217 **3.3. DOC versus CDOM for various types of waters**

218 **3.3.1 Freshwater lakes and reservoirs**

219 The relationship between DOC and CDOM has been investigated based on CDOM
220 absorption at different wavelengths (Fichot and Benner, 2011; Spencer et al., 2012;
221 Song et al., 2013; Brezonik et al., 2015). As suggested by Fichot and Benner (2011),
222 CDOM absorptions at 275 nm ($a_{CDOM(275)}$) and 295 nm ($a_{CDOM(295)}$) have stable
223 performances for DOC estimates for coastal waters. In current study, a strong
224 relationship ($R^2 = 0.85$) between DOC and $a_{CDOM(275)}$ was found in fresh lakes and
225 reservoirs (Fig.3a). However, the inclusion of $a_{CDOM(295)}$ explains very limited
226 variance, thus it is not considered in the regression models. Regression analyses of
227 water samples collected from different regions indicated that the slopes varied from
228 1.30 to 3.01 (Table 3). Water samples collected from East China and South China had

229 lower regression slope values (Table 3), and lakes and reservoirs were generally
230 mesotrophic or eutrophic (Huang et al., 2014; Yang et al., 2012, and references therein).

231 **[Insert Table 3 about here]**

232 **[Insert Fig.3 about here]**

233 ***3.3.2 Saline lakes***

234 A strong relationship between DOC and $a_{CDOM}(275)$ ($R^2 = 0.85$) was demonstrated for
235 saline lakes (Fig.3b) with much lower regression slope value (slope = 1.28). Further,
236 the regression slopes exhibited large variations in different regions (Table 3), ranging
237 from 0.86 in Tibetan waters to 2.83 in the Songnen Plain waters (see Fig.2 for location).
238 As the extreme case, the slope value was only 0.33 as demonstrated in the embedded
239 diagram in Fig.3b. Saline lakes in semi-arid or arid regions generally exhibit higher
240 regression slope values, for example, the west Songnen Plain (2.83), the Hulunbir
241 Plateau and the East Inner Mongolia Plateau (1.79). Whereas, waters in the west Inner
242 Mongolia Plateau (1.13), the Tibetan Plateau (0.86) exhibited low slope values (Table
243 3), and the extreme low value was measured in the Lake Qinhai in Tibetan Plateau.

244 ***3.3.3 Streams and rivers***

245 Although some of the samples scattered from the regression line (Fig.3c), close
246 relationship between DOC and $a_{CDOM}(275)$ was found for samples collected in rivers
247 and streams. Compared with the other water types (Fig.3), rivers and streams exhibited
248 the highest regression slope value (slope = 3.01). Further regression analysis with water
249 samples sub-datasets collected in different regions indicated that slope values presented
250 large variability, ranging from 1.07 to 8.49. The lower regression slope values were

251 recorded in water samples collected in rivers and stream in semi-arid and arid regions,
252 such as the Tibetan Plateau, Mongolia Plateau and Tarim Basin, while the higher values
253 were found in samples collected in streams originated from wetland and forest in
254 Northeast China (Table 3).

255 To investigate the dynamics of CDOM absorption and DOC concentrations, three
256 sections were investigated in three major rivers in Northeast China (see Figure S1 for
257 location). River flow exerted obvious effect on DOC and CDOM (Fig.4) and flood
258 impulse brought large amount of DOC and CDOM into river channels. The
259 relationships between DOC and $a_{CDOM}(275)$ in sections along three rivers in Northeast
260 China were demonstrated in Fig.5. The sampling point in the Yalu River is near the
261 river head source, thus strong relationship ($R^2=0.92$) was exhibited with large slope
262 (Fig.5a). The relationship between DOC and $a_{CDOM}(275)$ in the Songhua River at
263 Harbin City section was much scattered ($R^2=0.64$, Fig.5c). With respect to Fig.5b, it is
264 an in-between case ($R^2=0.82$). The sampling point was affected by effluent from
265 Baishan City, thus the coefficient of determination ($R^2= 0.822$) and the regression slope
266 (3.72) were lower than that from the Yalu River at Changbai point, while higher than
267 that from the Songhua River at Harbin point.

268 **[Insert Fig.4 and Fig.5 about here]**

269 **3.3.4 Urban waters**

270 As shown in Fig.3d, relatively close relationship between DOC and $a_{CDOM}(275)$ was
271 revealed in urban waters ($R^2= 0.71$, $p<0.001$). Similarly, regression slope values for
272 urban waters also changed remarkably, ranging from 0.87 to 2.45 (Table 3). High

273 nutrients in urban waters (Table 1) usually result in algal bloom in most urban water
274 bodies (Chl-a range: 1.0-521.1 $\mu\text{g/L}$; average: 38.9 $\mu\text{g/L}$), which might contribute the
275 high DOC concentrations in urban waters (Table 1). Thereby, the contribution from
276 algal decomposition and cell lysis to DOC and CDOM should not be neglected for
277 urban waters (Zhang et al., 2010; Zhao et al., 2016b; Zhou et al., 2016).

278 ***3.3.5 Ice covered lakes and reservoirs***

279 The closest relationship ($R^2 = 0.93$) between DOC and $a_{\text{CDOM}(275)}$ was recorded in
280 waters beneath ice covered lakes and reservoirs in Northeast China (Fig.3e).
281 Comparatively, a weak relationship between DOC and $a_{\text{CDOM}(275)}$ was demonstrated
282 in ice melting waters (Fig.3f). Apparently, CDOM from ice melting waters were mainly
283 originated from maternal water during the ice formation, also from algal biological
284 processes (Stedmon et al., 2011; Arrigo et al., 2010). Interestingly, the regression slopes
285 for ice samples (1.35) and under lying water sample (1.27) are very close. In addition,
286 there was a significant relationship between DOC in ice and underlying waters ($R^2 =$
287 0.86), indicating the dominant components of CDOM and DOC in the ice are from
288 maternal underlying waters.

289 ***3.3.6 DOC versus $a_{\text{CDOM}(440)}$***

290 CDOM absorption at 440 nm, i.e., $a_{\text{CDOM}(440)}$, is usually used as a surrogate to
291 represent its concentration (Bricaud et al., 1981; Babin et al., 2003), and widely used in
292 remote sensing community to quantify CDOM in waters (Lee et al., 2002; Binding et
293 al., 2008; Zhu et al., 2014). Significant relationships between DOC and $a_{\text{CDOM}(440)}$
294 were found in different types of waters (Fig.5). Through comparing Fig.3 with Fig.6, it

295 can be found that the overall relationships between DOC and CDOM at 440 nm
296 resembled that at 275 nm for different types of waters, but with relatively loose
297 relationship as indicated by the coefficients of determination (see Table S5).

298 **[Insert Fig.6 about here]**

299 **3.4 CDOM molecular weight and aromaticity versus DOC**

300 **3.4.1 CDOM versus SUVA₂₅₄ and M value ($a_{CDOM(250)}/a_{CDOM(365)}$)**

301 The large slope variations of regressions between DOC and $a_{CDOM(275)}$ in different
302 types of waters are probably due to the aromaticity and colored fractions in DOC
303 component (Spencer et al., 2009, 2012; Lee et al., 2015). As shown in Fig.7a, it can be
304 seen that SUVA₂₅₄ had high values in fresh lakes, and waters from rivers or streams as
305 well. Saline water and ice covered waters in Northeast China showed intermediate
306 SUVA₂₅₄ values, while urban water and ice melting water exhibited lower values. The
307 M value, i.e., $a_{CDOM(250)}/a_{CDOM(365)}$ is another indicator to demonstrate the variation
308 of molecular weight of CDOM components (De Haan, 1993). Compared to saline water,
309 fresh lake water (*t-Test*: $F = 631$, $p < 0.01$), river and stream water (*t-Test*: $F = 565$, $p <$
310 0.001), and urban water (*t-Test*: $F = 393$, $p < 0.001$) exhibited low M values (Fig.7b),
311 which indicated that large weight molecules dominate in these three types of waters.
312 Saline water, ice covered water in Northeast China and ice melting water showed higher
313 M values. Since SUVA₂₅₄ is a proxy based on the ratio to DOC, it is inappropriate to
314 establish the relationship between CDOM and DOC based on the SUVA₂₅₄
315 classification. Thereby, only M values, which reveal molecular weight and aromaticity,
316 might help to estimate DOC through CDOM absorption based on M values for various

317 types of waters.

318 **[Insert Fig.7 about here]**

319 ***3.4.2 Regression based on M values***

320 Regression models between DOC and $a_{CDOM}(275)$ were established based on M value
321 grouping. Four groups were achieved with hierarchical cluster approach, and each
322 group occupied about 44.74% ($M < 9.0$), 34.24% ($9.0 < M < 16.0$), 18.22% ($16.0 < M <$
323 25.0) and 2.80% ($25.0 < M < 68.0$) of the total samples from group 1 to 4, respectively.
324 Though only M values were used in the cluster which meant the feature space in
325 classification only had one dimension and the groups were mainly divided according to
326 the distribution of M values, the hierarchical cluster approach generated rational results.
327 As shown in Fig.8, a close relationship ($R^2 = 0.90$) between DOC and $a_{CDOM}(275)$ was
328 revealed in dataset where $M < 9.0$. Likewise, close relationship regression model
329 appeared in dataset with intermediate M values (Group 2 in Fig.8), revealing high
330 determination of coefficients ($R^2 = 0.91$). A relative weak relationship ($R^2 = 0.79$)
331 between DOC and $a_{CDOM}(275)$ appeared with M values ranging from 16.0 to 25.0. A
332 very close relationship ($R^2 = 0.98$) was found with extremely high M values (Group 4
333 in Fig.8).

334 As noted in Fig.8, close regression slopes implicated that a comprehensive
335 regression model with intermediate M values less than 16 may be achieved. As
336 expected, a promising regression model (the diagram was not shown) between DOC
337 and $a_{CDOM}(275)$ was achieved ($y = 1.269x + 6.42$, $R^2 = 0.909$, $N = 1171$, $p < 0.001$) with
338 pooled dataset in group 1 and group 2 shown in Fig.8. Inspired by this idea, the

339 relationship between $a_{CDOM}(275)$ and DOC also examined with pooled data. As shown
340 in Fig.9a, a significant relationship between DOC and $a_{CDOM}(275)$ was obtained with
341 the pooled dataset (N = 1504) collected from different types of inland waters. However,
342 it should be noted that the extremely high DOC samples may advantageously contribute
343 the better performance of the regression model. Thus, regression model excluding these
344 eight samples (DOC > 300 mg/L) was acceptable (Fig.9b, $R^2 = 0.51$, $p < 0.001$), but
345 greatly degraded. In addition, regression model with power function was established in
346 decimal logarithms log-log scale (Fig.9c, $R^2 = 0.77$, $p < 0.001$).

347 **[Insert Fig.8 and Fig.9 about here]**

348 **4. Discussion**

349 **4.1 Variation of water quality parameters**

350 Different water types were sampled across China with different climatic, hydrologic,
351 and land use conditions in various catchment, combined with different anthropogenic
352 intensity, thus the biological and geochemical properties in the water bodies are quite
353 diverse with large range values for each parameters (Table 1). Extremely turbid waters
354 are observed for fresh waters, saline waters and underlying waters covered by ice,
355 which were generally collected in very shallow water bodies in different parts of China.
356 As expected, large variations of Chl-a are observed for both fresh waters and urban
357 waters, and particularly these samples collected in urban waters show large range (1.0-
358 521.1 $\mu\text{g/L}$). Our investigation also indicates that algal growth is still very active in
359 these ice covered water bodies in Northeast China, which might result from high TN
360 ($4.3\pm 5.4\text{mg/L}$) and TP ($0.7\pm 0.6\text{mg/L}$) concentrations in these waters bodies. It also

361 should be noted that DOC, EC and pH were high in semi-arid or arid climatic regions,
362 which are consistent with previous findings (Curtis and Adams, 1995; Song et al., 2013;
363 Wen et al., 2016).

364 **4.2 DOC variation with different types of waters**

365 This investigation indicates that lower DOC were encountered with samples collected
366 in rivers from the Tibetan Plateau (Table 2), where the average soil organic matter is
367 lower, thus terrestrial DOC input from the catchment is less (Tian et al., 2008). However,
368 high DOC concentrations were found in rivers or streams surrounded by forest or
369 wetlands in Northeast China, the similar findings were also reported by Agren et al.
370 (2007, 2011). Further, lower DOC concentration is also measured with ice samples,
371 which is consistent with previous findings (Bezilie et al., 2002; Shao et al., 2016). But
372 relatively high DOC concentration was observed for underlying waters covered by ice
373 in Northeast China due to the condensed effect caused by the DOC discharged from ice
374 formation (Bezilie et al., 2002; Shao et al., 2016; Zhao et al., 2016a). This condensed
375 effect was particularly marked in these shallow water bodies where ice forming
376 remarkably condensed the DOC in the underlying waters (Zhao et al., 2016a). It also
377 should be noted that DOC concentration has a strong connection with hydrological
378 condition and catchment landscape features (Neff et al., 2006; Agren et al., 2007; Lee
379 et al., 2015). It should be noted that large DOC variations were observed in saline lakes
380 in different regions (Table 2). Much higher DOC concentrations were found in saline
381 lakes in Qinghai and Hulunbir, while relative low concentrations were observed in
382 Xilinguole Plateau and the Songnen Plain, which is consistent with previous

383 investigations conducted in the semi-arid or arid regions (Curtis and Adams, 1995;
384 Song et al., 2013; Wen et al., 2016).

385 **4.3 Variation of the relationships between CDOM and DOC**

386 As demonstrated in Fig.3, obvious variation is revealed for the regression slope values
387 between DOC and $a_{CDOM}(275)$. Most of the fresh water bodies are located in East China,
388 where agricultural pollution and anthropogenic discharge have resulted in serious
389 eutrophication (Tong et al., 2017). Phytoplankton degradation may contribute relative
390 large portion of CDOM and DOC in these water bodies (Zhang et al., 2010; Zhou et al.,
391 2016). Comparatively, fresh waters in Northeast and North China revealed larger
392 regression slopes (Table 3). Waters in Northeast China are surrounded by forest,
393 wetlands and grassland and therefore they generally exhibited high proportion of
394 colored fractions of DOC. Further, soils in Northeast China are rich in organic carbon,
395 which may also contribute to high concentration of DOC and CDOM in waters in this
396 region (Jin et al., 2016; Zhao et al., 2016a). Compared with waters in East and South
397 China, waters in Northeast China showed less algal bloom due to low temperature, thus
398 autochthonous CDOM was less presented in waters in Northeast China (Song et al.,
399 2013; Zhao et al., 2016a). As suggested by Brezonik et al. (2015) and Cardille et al.
400 (2013), CDOM in the eutrophic waters or those with very short resident time may show
401 seasonal variation due to algal bloom or hydrological variability, while CDOM in some
402 oligotrophic lakes or those with long resident time may show a stable pattern.

403 As shown in Fig.3b, smaller regression slope is revealed between DOC and
404 $a_{CDOM}(275)$ for saline waters, indicating less colored portion of DOC was presented in

405 waters in semi-arid to arid regions, especially for these closed lakes with enhanced
406 photochemical processes, enhanced by longer residence time and strong solar radiation
407 (Spencer et al., 2012; Song et al., 2013; Wen et al., 2016). The findings highlighted the
408 difference for the relationship between CDOM and DOC, thus different regression
409 models should be established to accurately estimate DOC in waters through linking
410 with CDOM absorption, particularly for fresh and saline waters that showing different
411 specific absorption coefficients (Song et al., 2013; Cardille et al., 2013; Brezonik et al.,
412 2015).

413 DOC concentration is strongly associated with hydrological conditions (Neff et al.
414 2006; Agren et al. 2007; Yu et al., 2016). The relationships between CDOM and DOC
415 in river and stream waters are very variable due to the hydrological variability and
416 catchment features (Agren et al., 2011; Spencer et al., 2012; Ward et al., 2013; Lee et
417 al., 2015; Zhao et al., 2017). As shown in Fig.4, the relationship between river flows
418 and DOC is rather complicated, which is mainly caused by the land use, soil properties,
419 relief, slope, the proportion of wetlands and forest, climate and hydrology of the
420 catchments (Neff et al., 2006; Sobek et al., 2007; Spencer et al., 2012; Zhou et al., 2016),
421 with additional influence by sewage discharge into rivers. The close relationship for
422 head waters with higher regression slope value (Fig.5a) is mainly attributed to that the
423 DOC and CDOM were fresh and less disturbed by pollution from anthropogenic
424 activities (Spencer et al., 2012; Shao et al., 2016). However, both point and non-point
425 source pollution complicated the relationship between DOC and DOM (Fig.5c).

426

427 **4.4 Regression models based on CDOM grouping**

428 As observed in Fig.3, the regression slopes (range: 0.33~3.01) for the relationship
429 between DOC and $a_{\text{CDOM}(275)}$ varied significantly. The CDOM absorption coefficient
430 is affected by its components and aromaticity, thus the M values are used to classify
431 CDOM into different groups, which turns to be an effective approach for improving
432 regression models (Fig.8) between DOC and $a_{\text{CDOM}(275)}$. It also should be highlighted
433 that the fourth group (Fig.8) is mainly from saline lakes (samples from embedded
434 diagram in Fig.3b), thus the regression model slope is extremely low. From the
435 regression model with pooled data, it can also be seen that relative accurate regression
436 model for CDOM versus DOC can be achieved with data collected in inland waters at
437 global scale (Sobek et al., 2007), which might be helpful in quantifying DOC through
438 linking with CDOM absorption, and the latter parameter can be estimated from remote
439 sensing data (Zhu et al., 2011; Kuster et al., 2015). Comparing Fig.8 and Fig.9b, it also
440 should be noted that some of the saline waters with extremely low CDOM absorption
441 efficiency (Group 4 in Fig.8) should be divided into different groups to achieve accurate
442 DOC regression model through CDOM absorption.

443 **5. Conclusions**

444 Based on the measurement of CDOM absorption and DOC laboratory analysis, we have
445 systematically examined the relationships between CDOM and DOC in various types
446 of waters in China. This investigation showed that CDOM absorption varied
447 significantly. River waters and fresh lake waters exhibited high CDOM absorption
448 values and specific CDOM absorption (SUVA_{254}). On the contrast, saline lakes

449 illustrated low $SUVA_{254}$ values probably due to the long residence time and strong
450 photo-bleaching effects on waters in the semi-arid regions.

451 The current investigation indicated that the relationships between CDOM
452 absorption and DOC varied remarkably by showing very varied regression slopes in
453 various types of waters. Head river water generally exhibits larger regression slope
454 values, while rivers affected by anthropogenic activities show lower slope values.
455 Saline water generally reveals small regression slope due to the photobleaching effect
456 in the semi-arid or arid region, combined with longer residence time. The accuracy of
457 regression model between $a_{CDOM}(275)$ and DOC was improved when CDOM
458 absorptions were divided into different sub-groups according to M values. Our finding
459 highlights that remote sensing models for DOC estimation based on the relationship
460 between CDOM and DOC should consider water types or cluster waters into several
461 groups according to their absorption features.

462

463 **Acknowledgements**

464 The authors would like to thank financial supports from the National Key Research and
465 Development Project (No. 2016YFB0501502), Natural Science Foundation of China
466 (No.41471290 and 41730104), and “One Hundred Talents” Program from Chinese
467 Academy of Sciences granted to Dr. Kaishan Song. Thanks are also extended to all the
468 staff and students for their efforts in field data collection and laboratory analysis, and
469 Dr. Hong Yang to review and polish the English language. The authors are greatly
470 indebted to associate Editor C. Stamm and these referees from both the previous and

471 the current versions of the manuscript for their very valuable comments that greatly
472 strengthened this manuscript.

473

474 **References**

475 Agren, A., Buffam, I., Jansson, M., Laudon, H., 2007. Importance of seasonality and
476 small streams for the landscape regulation of dissolved organic carbon export.
477 *Journal of Geophysical Research*, 112: G03003.

478 Agren, A., Haei, M., Kohler, S.J., Kohler, S.J., Bishop, K., Laudon, H., 2011.
479 Regulation of stream water dissolved organic carbon (DOC) concentrations during
480 snowmelt; the role of discharge, winter climate and memory effects.
481 *Biogeosciences*, 7, 2901-2913.

482 APHA/AWWA/WEF. 1998. Standard methods for the examination of water and
483 wastewater. Washington, DC: American Public Health Association.

484 Arrigo, K.R., Mock, T., Lizotte, M.P., 2010. Primary producers and sea ice, In *Sea Ice*,
485 edited by D.N. Thomas, and G.S. Dieckmann, pp. 283-326, second ed., Wiley-
486 Blackwell, Oxford, UK.

487 Babin, M., Stramski, D., Ferrari, G. M., Claustre, H., Bricaud, A., Obolensky, G.,
488 Hoepffner, N., 2003. Variations in the light absorption coefficients of
489 phytoplankton, nonalgal particles, and dissolved organic matter in coastal waters
490 around Europe. *Journal of Geophysical Research*, 108(C7), 3211.

491 Belzile, C., Gibson, J.A.E., Vincent, W.F., 2002. Colored dissolved organic matter and
492 dissolved organic carbon exclusion from lake ice: implications for irradiance

493 transmission and carbon cycling. *Limnology and Oceanography*, 47(5), 1283–
494 1293.

495 Binding, C.E., Jerome, J.H., Bukata, R.P., Booty, W.G., 2008. Spectral absorption
496 properties of dissolved and particulate matter in Lake Erie. *Remote Sensing of*
497 *Environment*, 112(4), 1702-1711.

498 Brezonik, P.L., Olmanson, L.G., Finlay, J.C., Bauer, M.E., 2015. Factors affecting the
499 measurement of CDOM by remote sensing of optically complex inland waters.
500 *Remote Sensing of Environment*, 157, 199-215.

501 Bricaud, A., Morel, A., Prieur, L., 1981. Absorption by dissolved organic matter of the
502 sea (yellow substance) in the UV and visible domains, *Limnology and*
503 *Oceanography*, 26(1), 43– 53.

504 Cardille, J.A., Leguet, J.B., del Giorgio, P., 2013. Remote sensing of lake CDOM using
505 noncontemporaneous field data. *Canadian Journal of Remote Sensing*, 39, 118–
506 126.

507 Chen, R.F., Bissett, P., Coble, P., Conmy, R., Gardner, G.B., Moran, M.A., Wang, X.C.,
508 Wells, M.L., Whelan, P., Zepp, R.G., 2004. Chromophoric dissolved organic
509 matter (CDOM) source characterization in the Louisiana Bight. *Marine Chemistry*,
510 89, 257-272.

511 Curtis, P.J., Adams, H.E., 1995. Dissolved organic matter quantity and quality from
512 freshwater and saltwater lakes in east-central Alberta. *Biogeochemistry* 30, 59–
513 76.

514 De Haan, H., 1993. Solar UV-light penetration and photodegradation of humic

515 substances in peaty lake water. *Limnology and Oceanography*, 1993, 38, 1072–
516 1076.

517 De Haan, H., De Boer, T., 1987. Applicability of light absorbance and fluorescence as
518 measures of concentration and molecular size of dissolved organic carbon in
519 humic Lake Tjeukemeer. *Water Research*, 21, 731–734.

520 Fichot, C.G., Benner, R., 2011. A novel method to estimate DOC concentrations from
521 CDOM absorption coefficients in coastal waters. *Geophysical Research Letter*,
522 38, L03610.

523 Findlay, S.E.G., Sinsbaugh, R.L., 2003. *Aquatic Ecosystems Interactivity of Dissolved*
524 *Organic Matter*. Academic Press, San Diego, CA, USA.

525 Gonnelli, M., Vestri, S., Santinelli, C., 2013. Chromophoric dissolved organic matter
526 and microbial enzymatic activity. A biophysical approach to understand the marine
527 carbon cycle. *Biophysical Chemistry*, 182, 79-85.

528 Helms, J.R., Stubbins, A., Ritchie, J.D., Minor, E.C., Kieber, D.J., Mopper, K., 2008.
529 Absorption spectral slopes and slope ratios as indicators of molecular weight,
530 source, and photobleaching of chromophoric dissolved organic matter. *Limnology*
531 *and Oceanography*, 53, 955–969.

532 Huang, C.C., Li, Y.M., Yang, H., Li, J.S., Chen, X., Sun, D.Y., Le, C.F., Zou, J., Xu,
533 L.J., 2014. Assessment of water constituents in highly turbid productive water by
534 optimization bio-optical retrieval model after optical classification. *Journal of*
535 *Hydrology*, 519, 1572–1583.

536 Jaffé, R., McKnight, D., Maie, N., Cory, R., McDowell, W.H., Campbell, J.L., 2008.

537 Spatial and temporal variations in DOM composition in ecosystems: The
538 importance of long-term monitoring of optical properties. *Journal of Geophysical*
539 *Research*, 113, G04032.

540 Jeffrey, S.W., Humphrey G.F., 1975. New spectrophotometric equations for
541 determining chlorophylls *a*, *b*, *c*₁, and *c*₂ in higher plants, algae and natural
542 phytoplankton. *Biochemie und Physiologie der Pflanzen*, 167(2), 191–194.

543 Jin, X.L., Du, J., Liu, H.J., Wang, Z.M., Song, K.S., 2016. Remote estimation of soil
544 organic matter content in the Sanjiang Plain, Northeast China: The optimal band
545 algorithm versus the GRA-ANN model. *Agricultural and Forest Meteorology*, 218,
546 250–260.

547 Kowalczyk, P., Zablocka, M., Sagan, S., Kulinski, K., 2010. Fluorescence measured in
548 situ as a proxy of CDOM absorption and DOC concentration in the Baltic Sea.
549 *Oceanologia*, 52(3), 431–471.

550 Kutser, T., Verpoorter, C., Paavel, B., Tranvik, L.J., 2015. Estimating lake carbon
551 fractions from remote sensing data. *Remote Sensing of Environment*, 157, 138–
552 146.

553 Lai, L., Huang, X., Yang, H., Chuai, X., Zhang, M., Zhong, T., Chen, Z., Chen, Y.,
554 Wang, X., Thompson, J.R., 2016. Carbon emissions from land-use change and
555 management in China between 1990 and 2010. *Science Advances*, 2(11),
556 e1601063.

557 Le, C.F., Hu, C.M., Cannizzaro, J., Duan, H.T., 2013. Long-term distribution patterns
558 of remotely sensed water quality parameters in Chesapeake Bay. *Estuarine*,

559 Coastal and Shelf Science, 128(10), 93–103.

560 Lee, E.J., Yoo, G.Y., Jeong, Y., Kim, K.U., Park, J.H., Oh, N.H., 2015. Comparison of
561 UV–VIS and FDOM sensors for in situ monitoring of stream DOC concentrations.
562 Biogeosciences, 12, 3109–3118.

563 Lee, Z.P., Carder, K.L., Arnone, R.A., 2002. Deriving inherent optical properties from
564 water color: A multiband quasi-analytical algorithm for optically deep waters.
565 Applied Optics, 41(27), 5755–5777.

566 Miller, W.L., Zepp, R.G., 1995. Photochemical production of dissolved inorganic
567 carbon from terrestrial organic matter: Significance to the oceanic organic carbon
568 cycle. Geophysical Research Letter, 22 (4), 417–420.

569 Neff, J.C., Finlay, J.C., Zimov, S.A., Davydov, S.P., Carrasco, J.J., Schuur, E.A.G.,
570 Davydova, A.I., 2006. Seasonal changes in the age and structure of dissolved
571 organic carbon in Siberian rivers and streams. Geophysical Research Letter, 33,
572 L23401.

573 Pekel, J.F., Cottam, A., Gorelick, N., Belward, A.S., 2016. High-resolution mapping of
574 global surface water and its long-term changes. Nature, 540, 417–422.

575 Raymond, P. A., Hartmann, J., Lauerwarld, R., et al., 2013. Global carbon dioxide
576 emissions from inland waters. Nature, 503(7476), 355–359.

577 Reche, I., Pace, M., Cole, J.J., 1999. Relationship of trophic and chemical conditions
578 to photobleaching of dissolved organic matter in lake ecosystems.
579 Biogeochemistry, 44, 529–280.

580 Shao, T.T., Song, K.S., Du, J., Zhao, Y., Ding, Z., Guan, Y., Liu, L., Zhang, B., 2016.

581 Seasonal variations of CDOM optical properties in rivers across the Liaohe Delta.
582 Wetlands, 36 (suppl.1): 181–192.

583 Shi, K., Li, Y., Li, L., et al., 2013. Remote chlorophyll-a estimates for inland waters
584 based on a cluster-based classification. Science of the Total Environment, 444, 1–
585 15.

586 Spencer, R.G.M., Stubbins, A., Hernes, P.J., Baker, A., Mopper, K., Aufdenkampe,
587 A.K., Dyda, R.Y., Mwamba, V.L., Mangangu, A.M., Wabakanghanzi, J.N., Six,
588 J., 2009. Photochemical degradation of dissolved organic matter and dissolved
589 ligninphenols from the Congo River. Journal of Geophysical Research, 114,
590 G03010.

591 Spencer, R.G.M., Butler, K.D., Aiken, G.R., 2012. Dissolved organic carbon and
592 chromophoric dissolved organic matter properties of rivers in the USA. Journal
593 of Geophysical Research, 117, G03001.

594 Sobek, S., Tranvik, L.J., Prairie, Y.T., Kortelainen, P., Cole, J.J., 2007. Patterns and
595 regulation of dissolved organic carbon: An analysis of 7,500 widely distributed
596 lakes. Limnology and Oceanography 52, 1208–1219.

597 Song, K.S., Zang, S.Y., Zhao, Y., Li, L., Du, J., Zhang, N.N., Wang, X.D., Shao, T.T.,
598 Liu, L., Guan, Y., 2013. Spatiotemporal characterization of dissolved Carbon for
599 inland waters in semi-humid/semiarid region, China. Hydrology and Earth
600 System Science, 17, 4269–4281.

601 Stedmon, C.A., Thomas, D.N., Papadimitriou, S., Granskog, M.A., Dieckmann, G.S.
602 2011. Using fluorescence to characterize dissolved organic matter in Antarctic

603 sea ice brines. *Journal of Geophysical Research*, 116, G03027.

604 Tian, Y.Q., Ouyang, H., Xu, X.L., Song, M.H., Zhou, C.P., 2008. Distribution
605 characteristics of soil organic carbon storage and density on the Qinghai-Tibet
606 Plateau. *Acta Pedologica Sinica*, 45(5), 933–942. (In Chinese with English
607 abstract).

608 Tong, Y.D., Zhang, W., Wang, X.J., et al., 2017. Decline in Chinese lake phosphorus
609 concentration accompanied by shift in sources since 2006. *Nature Geoscience*,
610 10(7), 507–511.

611 Tranvik, L.J., Downing, J.A., Cotner, J.B., et al., 2009. Lakes and reservoirs as
612 regulators of carbon cycling and climate. *Limnology and Oceanography*, 54(6),
613 2298–2314.

614 Vantrepotte, V., Loisel, H., Dessailly, D., et al., 2012. Optical classification of
615 contrasted coastal waters. *Remote Sensing of Environment*, 123, 306–323.

616 Verpoorter, C., Kutser, T., Seekell, D.A., Tranvik, L.J., 2014. A global inventory of
617 lakes based on high-resolution satellite imagery. *Geophysical Research Letter*, 41,
618 6396–6402.

619 Vodacek, A., Blough, N.V., Degrandpre, M.D., Peltzer, E.T., Nelson, R.K., 1997.
620 Seasonal variation of CDOM and DOC in the Middle Atlantic Bight: terrestrial
621 inputs and photooxidation. *Limnology and Oceanography*, 42, 674–686.

622 Ward Jr, J.H., 1963. Hierarchical grouping to optimize an objective function. *Journal of*
623 *the American Statistical Association*, 58(301), 236–244.

624 Ward, N.D., Keil, R.G., Medeiros, P.M., Brito, D.C., Cunha, A.C., Dittmar, T., Yager,

625 P.L., Krusche, A.V. and Richey, J.E., 2013. Degradation of terrestrially derived
626 macromolecules in the Amazon River. *Nature Geoscience*, 6(7), 530–533.

627 Weishaar, J.L., Aiken, G.R., Bergamaschi, B.A., Fram, M.S., Fugii, R., Mopper, K.,
628 2003. Evaluation of specific ultraviolet absorbance as an indicator of the chemical
629 composition and reactivity of dissolved organic carbon. *Environmental Science
630 and Technology*, 37, 4702–4708.

631 Wen, Z.D., Song, K.S., Zhao, Y., Du, J., Ma, J.H., 2016. Influence of environmental
632 factors on spectral characteristic of chromophoric dissolved organic matter
633 (CDOM) in Inner Mongolia Plateau, China. *Hydrology and Earth System
634 Sciences*, 20, 787–801.

635 Williamson, C.E., Rose, K.C., 2010. When UV meets fresh water. *Science*, 329, 637–
636 639.

637 Wilson, H., Xenopoulos, M.A., 2008. Ecosystem and seasonal control of stream
638 dissolved organic carbon along a gradient of land use. *Ecosystems* 11, 555–568.

639 Yang, H., Andersen, T., Dörsch, P., Tominaga, K., Thrane, J.-E., Hessen, D. O., 2015.
640 Greenhouse gas metabolism in Nordic boreal lakes. *Biogeochemistry*, 126, 211–
641 225.

642 Yang, H., Xie, P., Ni, L., Flower, R. J., 2012. Pollution in the Yangtze. *Science*, 337,
643 (6093), 410-410.

644 Yu, Q., Tian, Y. Q., Chen, R.F., Liu, A., Gardner, G.B., Zhu, W.N., 2010. Functional
645 linear analysis of in situ hyperspectral data for assessing CDOM in
646 rivers. *Photogrammetric Engineering & Remote Sensing*, 76(10), 1147–1158.

647 Yu, X.L., Shen, F., Liu, Y.Y., 2016. Light absorption properties of CDOM in the
648 Changjiang (Yangtze) estuarine and coastal waters: An alternative approach for
649 DOC estimation. *Estuarine, Coastal and Shelf Science*, 181, 302–311.

650 Zhang, Y.L., Zhang, E.L., Yin, Y., Van Dijk, M.A., Feng, L.Q., Shi, Z.Q., Liu, M.L.,
651 Qin, B.Q., 2010. Characteristics and sources of chromophoric dissolved organic
652 matter in lakes of the Yungui Plateau, China, differing in trophic state and altitude.
653 *Limnology and Oceanography*, 55(6), 2645–2659.

654 Zhao, Y., Song, K.S., Wen, Z.D., Li, L., Zang, S.Y., Shao, T.T., Li, S.J., Du, J., 2016a.
655 Seasonal characterization of CDOM for lakes in semiarid regions of Northeast
656 China using excitation–emission matrix fluorescence and parallel factor analysis
657 (EEM - PARAFAC). *Biogeosciences*, 13, 1635–1645.

658 Zhao, Y., Song, K.S., Li, S.J., Ma, J.H., Wen, Z.D., 2016b. Characterization of CDOM
659 from urban waters in Northern-Northeastern China using excitation-emission
660 matrix fluorescence and parallel factor analysis. *Environmental Science and
661 Pollution Research*, 23, 15381–15394.

662 Zhao, Y., Song, K.S., Shang, Y. X., Shao, T. T., Wen, Z.D., Lv, L.L., 2017.
663 Characterization of CDOM of river waters in China using fluorescence excitation-
664 emission matrix and regional integration techniques. *Journal of Geophysical
665 Research, Biogeoscience*, DOI: 10.1002/2017JG003820.

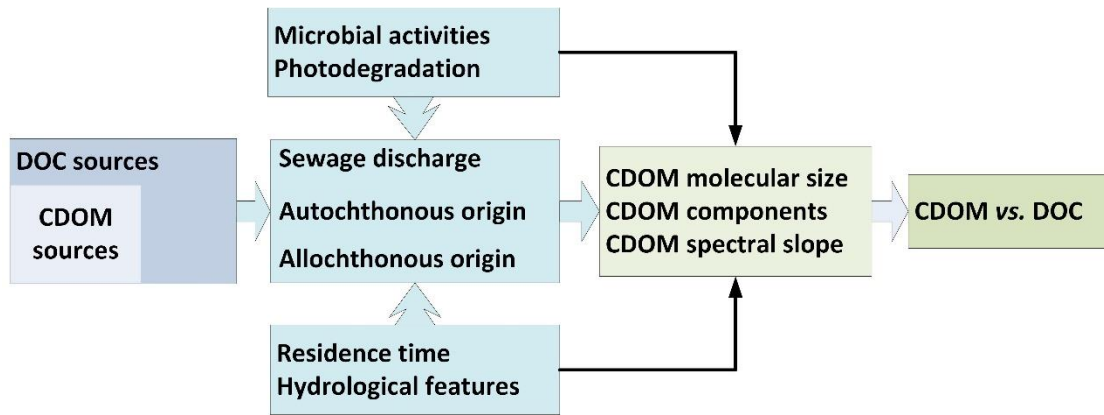
666 Zhou Y., Zhang Y., Jeppesen E., Murphy K.R., Shi K., Liu M., Liu X., Zhu G. Inflow
667 rate-driven changes in the composition and dynamics of chromophoric dissolved
668 organic matter in a large drinking water lake. *Water Research*, 2016, 100, 211-221.

669 Zhu, W., Yu, Q., Tian, Y. Q., Chen, R.F., Gardner, G.B., 2011. Estimation of
670 chromophoric dissolved organic matter in the Mississippi and Atchafalaya river
671 plume regions using above-surface hyperspectral remote sensing. *Journal of*
672 *Geophysical Research: Oceans* (1978–2012), 116(C2), C02011.

673 Zhu, W.N., Yu, Q., Tian, Y. Q., et al., 2014. An assessment of remote sensing algorithms
674 for colored dissolved organic matter in complex freshwater environments. *Remote*
675 *Sensing of Environment*, 140, 766-778.

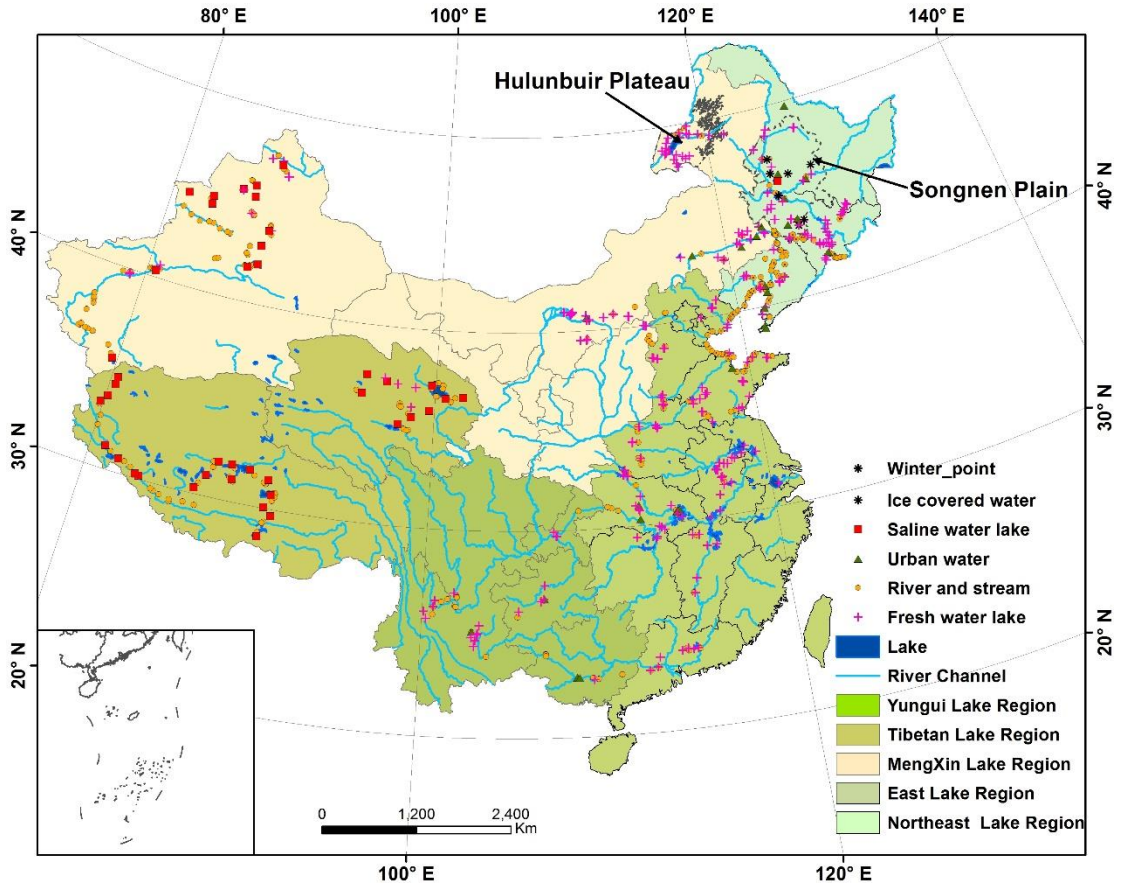
676 **Figures**

677 Fig.1. The potential regulating factors that influence the relationship between CDOM
678 and DOC. Note, CDOM sources are a subset of DOC sources, and hydrological feature
679 includes flow discharge, drainage area, catchment landscape, river level, and inflow or
680 outflow regions.



681
682
683
684
685
686
687
688
689
690
691
692
693
694
695
696
697
698
699

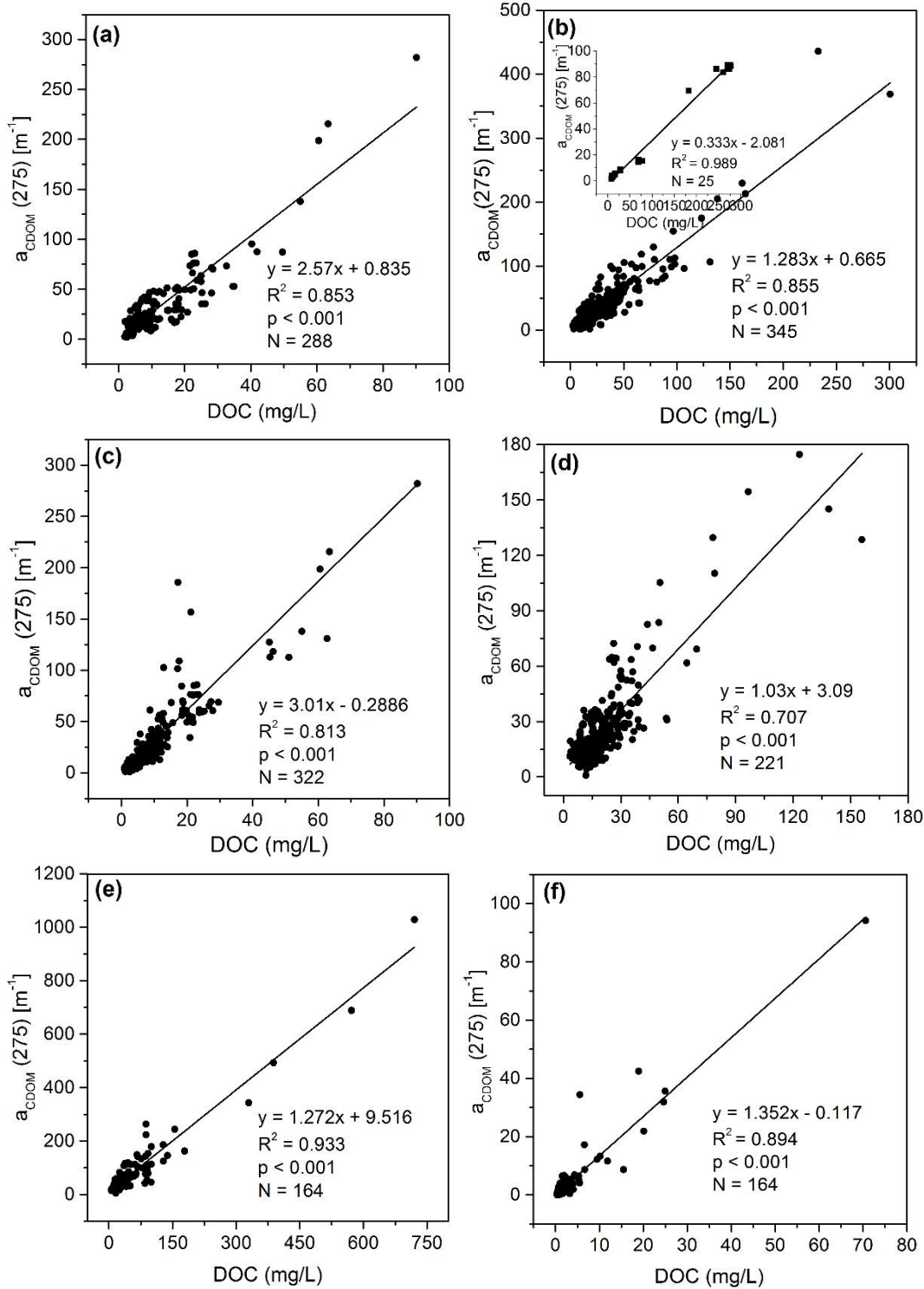
700 Fig.2. Water types and sample distributions across the mainland China. The dash line
 701 shows the boundary of some typical geographic units (i.e., Songnen Plain, and
 702 Hulunbuir Plateau).



703
 704
 705
 706
 707
 708
 709
 710
 711
 712
 713
 714
 715
 716
 717
 718

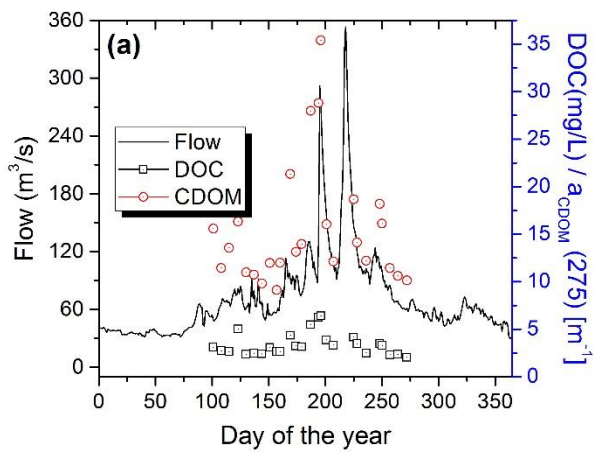
719 Fig.3. Relationship between DOC and $a_{CDOM}(275)$ in different types of inland waters,
 720 (a) fresh water lakes, (b) saline water lakes, (c) river and stream waters, (d) urban waters,

721 (e) ice covered lake underlying waters, and (f) ice melting lake waters.

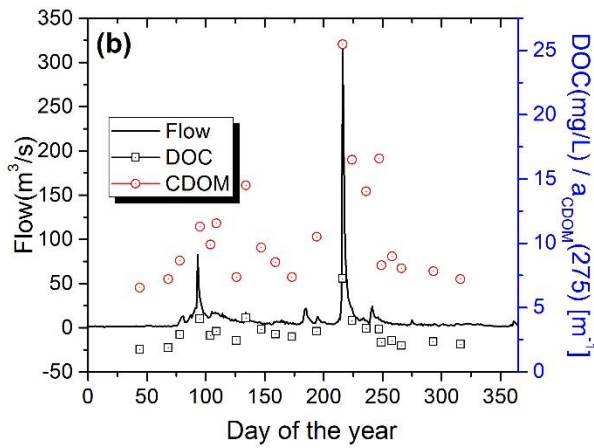


728 Fig.4. Concurrent flow dynamics for three rivers in Northeast China and the
 729 corresponding DOC and CDOM variations in 2015; (a) the Yalu River near Changbai

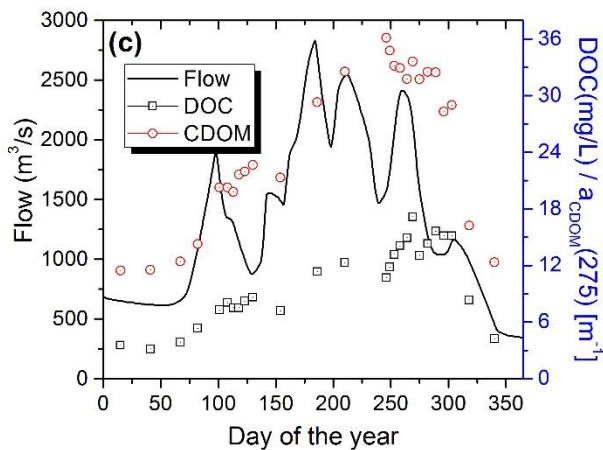
730 County, (b) the Hunjiang River with DOC and CDOM sampled at Baishan City, while
 731 the river flow gauge station is near the Tonghua City, (c) the Songhua River at Harbin
 732 City.



733



734



735

736

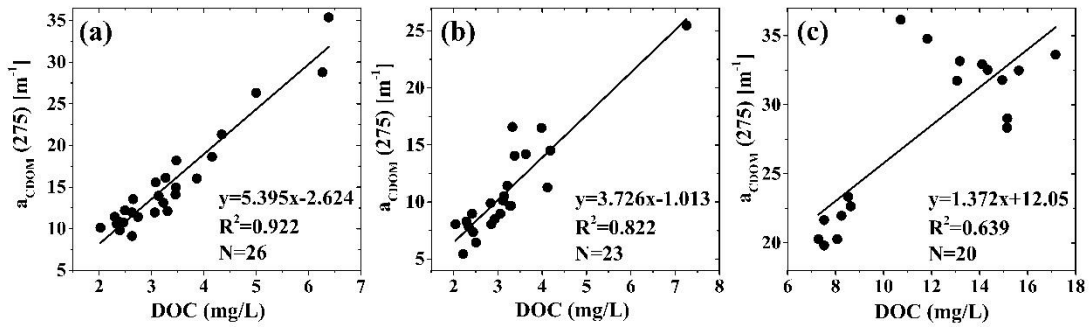
737

738

739 Fig.5. The relationships between $a_{CDOM}(275)$ and DOC at sections across (a) the Yalu
 740 River, (b) the Hunjiang River, and (c) the Songhua River. The samples were collected

741 at each station at about one week or around ten days in ice free season in 2015.

742



743

744

745

746

747

748

749

750

751

752

753

754

755

756

757

758

759

760

761

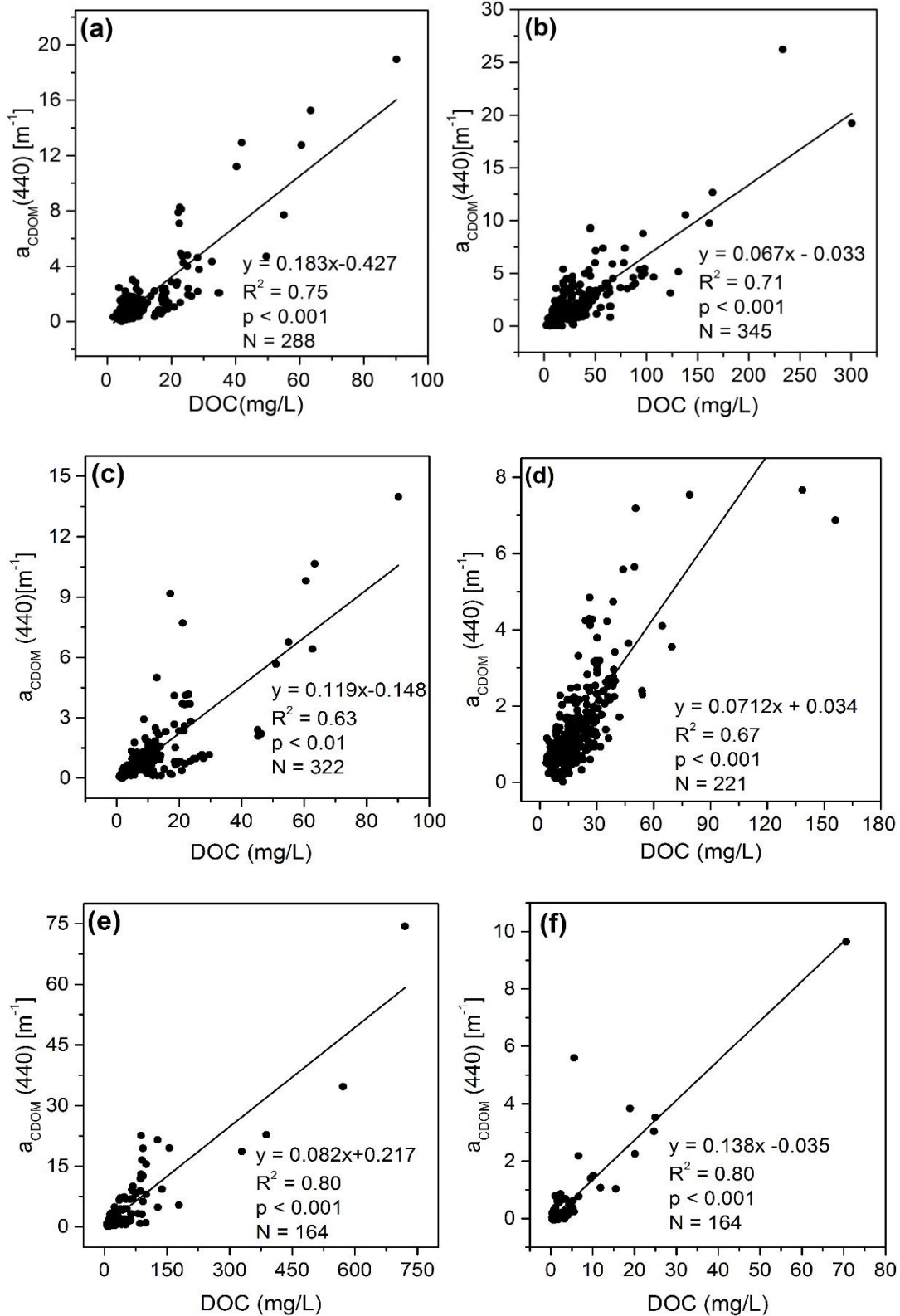
762

763

764 Fig.6. Relationship between DOC and $a_{CDOM}(440)$ in different types of inland waters,

765 (a) fresh water lakes, (b) saline water lakes, (c) river and stream waters, (d) urban waters,

766 (e) ice covered lake underlying waters, and (f) ice melting waters.



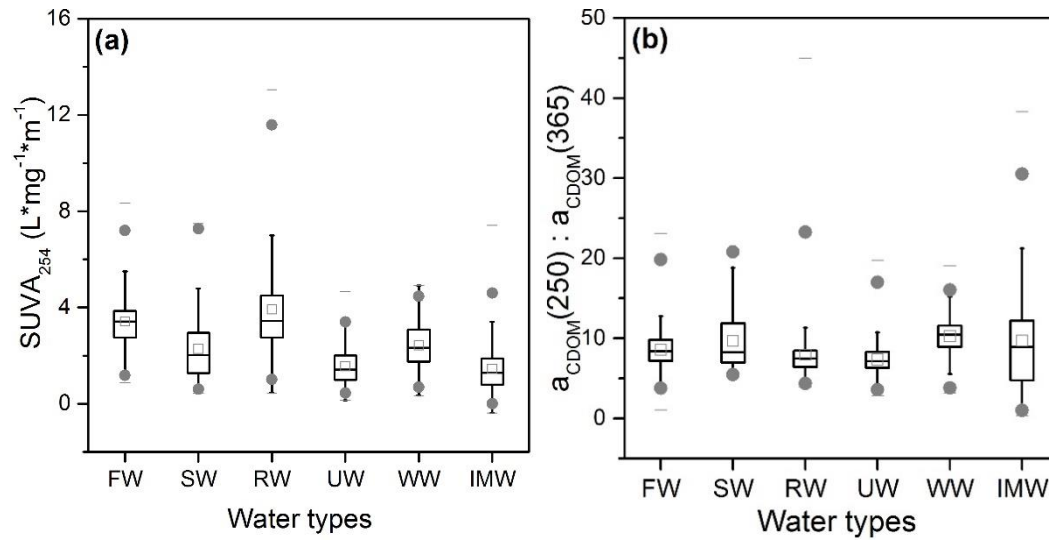
769

770

771 Fig.7. Comparison of (a) SUVA_{254} , and (b) M values ($a_{\text{CDOM}}(250) / a_{\text{CDOM}}(365)$) in

772 various types of inland waters. FW, fresh lake water; SW, saline lake water, RW, river

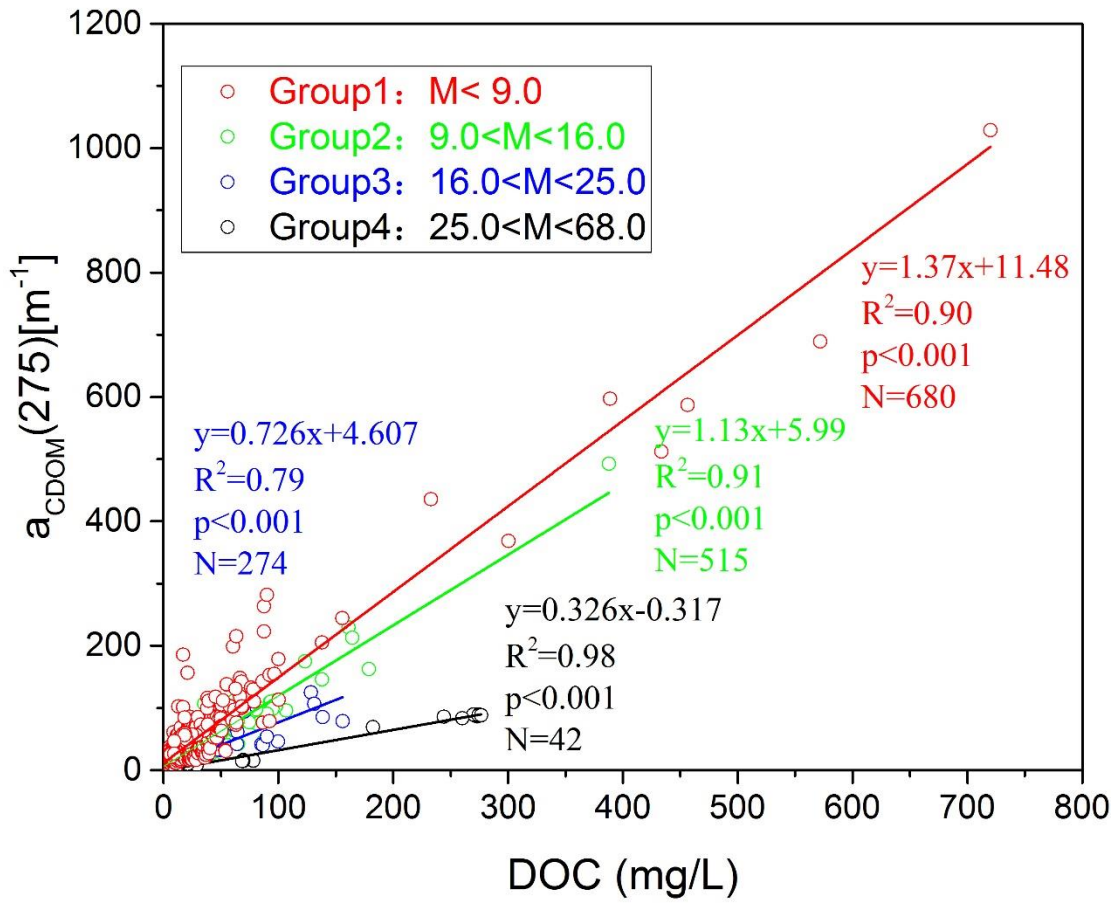
773 or stream water; UW, urban water; WW, ice covered waters from Northeast China; IMW,
 774 ice melt waters from Northeast China.



775
 776
 777
 778
 779
 780
 781
 782
 783
 784
 785
 786
 787
 788
 789
 790
 791
 792
 793
 794
 795
 796
 797
 798
 799

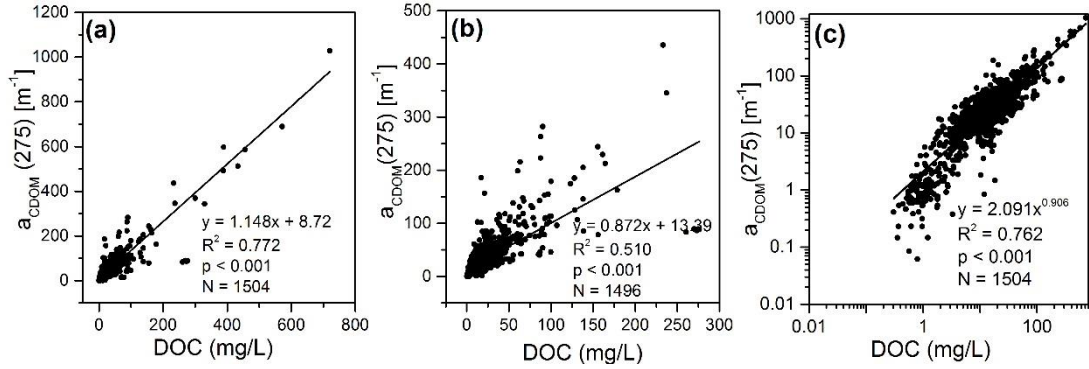
800 Fig.8. Relationship between DOC and a_{CDOM}275 sorted by M (a_{CDOM}(250)/a_{CDOM}(365))
 801 values, Group 1: M <9.0; Group 2: 9.0 < M <16.0; Group 3: 16.0 < M < 25.0; Group 4:

802 25.0 < M < 68.0.



803
804
805
806
807
808
809
810
811
812
813
814
815
816

817 Fig.9. the relationships between $a_{CDOM}(275)$ and DOC concentrations, (a) regression
818 model with pooled dataset; (b) regression model with DOC concentration less than 300
819 mg/L; (c) regression model with power fitting function based on log-log scale.



820

821

822

823

824

825

826

827

828

829

830

831

832

833

834

835

836 **Tables**

837

838 Table 1. Water quality in different types of waters, DOC, dissolved organic carbon; EC,
 839 electrical conductivity; TP, total phosphorus; TN, total nitrogen; TSM, total suspended
 840 matter; Chl-a, chlorophyll-a concentration.

		DOC (mg/L)	EC μs/cm	pH	TP (mg/L)	TN (mg/L)	TSM (mg/L)	Chl-a (μg/L)
FW	Mean	10.2	434.0	8.2	0.5	1.6	67.8	78.5
	Range	1.9-90.2	72.7-1181.5	6.9-9.3	0.01-10.4	0.001-9.5	0-1615	1.4-338.5
SW	Mean	27.3	4109.4	8.6	0.4	1.4	115.7	9.0
	Range	2.3-300.6	1067-41000	7.1-11.4	0.01-6.3	0.6-11.0	1.4-2188	0-113.7
RW	Mean	8.3	10489.1	7.8-9.5	-	-	-	-
	Range	0.9-90.2	3.7-1000	8.6	-	-	-	-
UW	Mean	19.44	525.4	8.0	3.4	3.5	50.5	38.9
	Range	3.5-123.3	28.6-1525	6.4-9.2	0.03-32.4	0.04-41.9	1-688	1.0-521.1
WW	Mean	67.0	1387.6	8.1	0.7	4.3	181.5	7.3
	Range	7.3-720	139-15080	7.0-9.7	0.1-4.8	0.5-48	9.0-2174	1.0-159.4
IMW	Mean	6.7	242.8	8.3	0.19	1.1	17.4	1.1
	Range	0.3-76.5	1.5-4350	6.7-10	0.02-2.9	0.3-8.6	0.3-254.6	0.28-5.8

841

842 Note: FW, fresh water lake; SW, saline water lake, RW, river or stream water; UW, urban water;

843 WW, ice covered winter water from Northeast China; IMW, ice melt water from Northeast China.

844

845

846

847

848

849

850

851

852

853

854

855

856

857

858

859

860 Table 2. Descriptive statistics of dissolved organic carbon (DOC) and $a_{CDOM}(440)$ in
 861 various types of waters. Min, minimum; Max, maximum; S.D, standard deviation.

862

Type	Region	DOC (mg/L)				$a_{CDOM}(440)$ [m^{-1}]			
		Min	Max	Mean	S.D	Min	Max	Mean	S.D
River	Liaohe	3.6	48.2	14.3	9.49	0.46	3.68	0.92	0.58
	Qinghai	1.2	8.5	4.4	1.96	0.13	2.11	0.54	0.63
	Inner Mongolia	16.9	90.2	40.4	24.84	0.32	7.46	1.03	2.11
	Songhua	0.9	21.1	8.1	4.96	0.32	18.93	3.2	4.19
Saline	Qinghai	1.7	130.9	67.9	56.7	0.13	0.86	0.36	0.23
	Hulunbir	8.4	300.6	68.5	69.2	0.82	26.21	4.41	4.45
	Xilinguole	3.74	45.4	14.2	8.8	0.36	4.7	1.34	0.88
	Songnen	3.6	32.6	16.4	7.4	0.46	33.80	2.4	3.78

863

864

865

866

867

868

869

870

871

872

873

874

875

876

877

878

879

880

881

882

883

884

885

886

887

888 Table 3. Fitting equations for DOC against $a_{CDOM}(275)$ in different types of waters
 889 except ice covered lake underlying water and ice melting waters.

Water types	Region or Basin	Equations	R ²	N
Freshwater lakes	Northeast Lake Region	$y = 3.13x - 3.438$	0.87	102
	MengXin Lake Region	$y = 2.16x - 1.279$	0.90	63
	East Lake Region	$y = 1.98x + 7.813$	0.66	69
	Yungui Lake Region	$y = 1.295x - 44.56$	0.71	54
Saline lakes	Songnen Plain	$y = 2.383x + 1.101$	0.92	159
	East Mongolia	$y = 1.791x + 8.560$	0.67	57
	West Mongolia	$y = 1.133x + 3.900$	0.81	46
	Tibetan Lake Region	$y = 0.864x + 2.255$	0.84	83
Rivers or streams	Branch of the Nenjiang River	$y = 7.655x - 42.64$	0.81	33
	Songhua River stem	$y = 3.759x - 6.618$	0.71	29
	Branch of Songhua River	$y = 8.496x - 12.14$	0.98	33
	Liao River Autumn 2012	$y = 1.099x + 3.900$	0.80	38
	Liao River Autumn 2013	$y = 1.073x - 4.157$	0.88	28
	Rivers from North China	$y = 3.154x - 1.207$	0.87	48
	Rivers from East China	$y = 3.037x - 2.585$	0.88	47
	Rivers from Tibetan Plateau	$y = 2.345x + 2.375$	0.87	41
Urban waters	Waters from Changchun	$y = 2.471x - 2.231$	0.54	48
	Waters from Harbin	$y = 1.413x - 4.521$	0.67	31
	Waters from Beijing	$y = 0.874x + 11.12$	0.63	27
	Waters from Tianjin	$y = 0.994x + 7.368$	0.57	23

890
 891
 892